Journal of Materials Chemistry A



PAPER

View Article Online
View Journal | View Issue



Cite this: J. Mater. Chem. A, 2015, 3, 13483

Solution-phase synthesis and thermal conductivity of nanostructured CdSe, In₂Se₃, and composites thereof†

Yuanyu Ma, a Minglu Liu, b Abbas Jaber and Robert Y. Wang*ab

The use of nanoparticle-in-matrix composites is a common motif among a broad range of nanoscience applications and is of particular interest to the thermal sciences community. To explore this morphological theme, we create crystalline inorganic composites with nanoparticle volume fractions ranging from 0 to ~100% using solution-phase processing. We synthesize these composites by mixing colloidal CdSe nanocrystals and In₂Se₃ metal-chalcogenide complex (MCC) precursor in the solutionphase and then thermally transform the MCC precursor into a crystalline In₂Se₃ matrix. We find rich structural and chemical interactions between the CdSe nanocrystals and the In₂Se₃ matrix, including alterations in In₂Se₃ grain size and orientation as well as the formation of a ternary phase, CdIn₂Se₄. The average thermal conductivities of the 100% In_2Se_3 and $\sim100\%$ CdSe composites are 0.32 and 0.53 W m⁻¹ K⁻¹, respectively. These thermal conductivities are remarkably low for inorganic crystalline materials and are comparable to amorphous polymers. With the exception of the \sim 100% CdSe samples, the thermal conductivities of these nanocomposites are insensitive to CdSe volume fraction and are \sim 0.3 W m⁻¹ K⁻¹ in all cases. We attribute this insensitivity to competing effects that arise from structural morphology changes during composite formation. This insensitivity to CdSe volume fraction also suggests that very low thermal conductivities can be reliably achieved using this solution-phase route to nanocomposites.

Received 15th April 2015 Accepted 22nd May 2015

DOI: 10.1039/c5ta02755a

www.rsc.org/MaterialsA

Introduction

Nanoparticle composites are a morphological theme spanning applications in thermoelectrics, ¹⁻⁷ thermal storage, ^{8,9} optoelectronics, ^{10,11} memory, ^{12,13} and smart windows. ^{14,15} Solution phase processes are a promising fabrication route to such composites because they utilize mild temperatures, moderate pressures, and inexpensive equipment, which generally lead to cost reductions. In addition, solution-phase processes provide a modular route wherein pre-synthesized colloidal nanostructures and matrices can be mixed in the solution-phase and then converted into a solid-phase nanocomposite. This approach has been commonly used to embed colloidal nanocrystals into polymers, ^{9,16,17} oxides, ^{18–20} semiconductors, ^{21,22} and metals. ⁸ Embedding colloidal nanocrystals into polymer matrices is generally straightforward because both of these materials are commonly soluble in a variety of solvents. On the

Metal-chalcogenide complexes (MCCs) have been demonstrated to be soluble precursors for a broad range of metalchalcogenide materials such as tin, indium, antimony, germanium, gallium, mercury, copper, and zinc chalcogenides. 21,23-26 These MCCs can also be used to replace the conventional organic ligands that passivate the surface of colloidal nanocrystals.21,22 MCCs used in this manner fall under the growing class of inorganic ligands for colloidal nanocrystals.27 This class includes MCCs,21 metal-free chalcogenides,28 polyoxometallates, 20 halide, pseudohalide and halometallates. 29 The use of these inorganic ligands as led to greatly improved charge transport mobilities in colloidal nanocrystal materials on the order of 10¹ cm² V⁻¹ s⁻¹. Promisingly, very recent work using CdSe nanocrystals functionalized with cadmium chalcogenidometallates has led to record mobility values on the order of 10^2 cm² V⁻¹ s⁻¹ and are within a factor of \sim 2 relative to single-crystal mobilities.35 This running theme of inorganic ligands has led to works on colloidal nanocrystal routes to transistors and integrated circuits, 33,36 photovoltaics, 37 smart windows,14 and thermoelectrics.31,38-42

other hand, inorganic matrices such as oxides, semiconductors, and metals are generally insoluble. This hurdle can be circumvented by identifying a soluble matrix precursor that can be mixed with colloidal nanocrystals and then converted into a solid inorganic matrix afterwards.

[&]quot;Materials Science & Engineering, Arizona State University, USA. E-mail: rywang@asu. edu

^bMechanical Engineering, Arizona State University, USA

[†] Electronic supplementary information (ESI) available: Experimental materials and method details, calculations for XRD peak intensity and Cahill–Pohl model, and additional figures with XRD, thermal conductivity, EDX, and RBS data. See DOI: 10.1039/c5ta02755a

One attractive trait of colloidal nanocrystals with MCC ligands is that by annealing them, the MCC ligands can be transformed into an ultrathin metal–chalcogenide layer between the nanocrystals, 21,22,34,42,43 thereby creating nanocomposites with an $\sim\!100\%$ nanoparticle volume fraction. In addition, the large variety of colloidal nanocrystal and MCC choices enables excellent control over nanocomposite parameters such as nanoparticle size and composition as well as matrix composition.

Inspired by this approach to nanocomposite fabrication, we explore the use of this chemistry to control an additional and important nanocomposite variable, that of nanoparticle volume fraction. By varying the colloidal nanocrystal-MCC precursor ratio in solution prior to nanocomposite formation, we create composites with nanoparticle volume fractions ranging from 0 to ~100%. Although such control over nanoparticle volume fraction has been previously demonstrated, few characterization details were reported.21 In this work, we combine CdSe nanocrystals with varying amounts of In₂Se₃ MCC precursor and then characterize the resulting composites with X-ray diffraction (XRD), transmission electron microscopy (TEM), scanning electron microscopy (SEM), Rutherford backscattering spectroscopy (RBS), particle-induced X-ray emission (PIXE), and energy dispersive X-ray spectroscopy (EDX). This work complements earlier works on CdSe nanocrystals with In₂Se₃ MCCs that focused on very high nanocrystal volume fractions, but did not otherwise explore the dimension of nanoparticle volume fraction.34,44

The structural motif of nanoparticles embedded in a crystalline matrix is a common theme in the thermal science community. 1-5,7,45,46 In particular, it is well known that matrixembedded nanoparticles promote broadband scattering of phonons, which correspondingly leads to low thermal conductivities. This is particularly important for thermoelectric applications wherein reduced thermal conductivities lead to large improvements in energy conversion efficiency. 1-5,7 This paper's solution-phase synthesis approach contrasts with many of the recent materials processes used to create nanostructured thermoelectrics such as molecular beam epitaxy,5 ball-milling/hotpressing, 47,48 melt-processing, 7 and melt-processing/power-processing/spark-plasma-sintering.1 In particular, the use of colloidal nanocrystals enables precise size control over the nanoparticle inclusions that is not possible by these other processing approaches. Furthermore, recent computational work suggests that the best nanoparticle size distribution for minimum thermal conductivity is neither a narrowly monodisperse or broadly polydisperse diameter distribution.49 Instead the optimal size distribution consists of a mixture of several different monodisperse diameters. 49 Composites such as this could be achieved by mixing together colloidal nanocrystals of different diameters. It should also be noted that a recent cost-analysis on thermoelectric materials manufacturing suggests that solution-phase processing could lead to significant cost improvements relative to typical thermoelectric materials processing. 50

Due to the importance of this nanoparticle-in-matrix structural motif to the thermal science community, we measured the thermal conductivity of our nanoparticle-in-matrix composites as a function of nanoparticle volume fraction. We find that the thermal conductivity of the CdSe-In₂Se₃ composites is very low over the entire nanoparticle volume fraction range. The average thermal conductivity of the \sim 100% CdSe composites is 0.53 W m⁻¹ K⁻¹, which is 17 times lower than bulk single crystal CdSe.51,52 The average thermal conductivity of the 100% In2Se3 composites is 0.32 W m⁻¹ K⁻¹, which is 3 times lower than other literature results on polycrystalline In2Se3.53 With the exception of the \sim 100% CdSe sample, the thermal conductivities of these nanocomposites are insensitive to CdSe volume fraction. We believe this insensitivity is due to competing effects that both increase and decrease the composite's thermal conductivity. Many of these competing effects arise from changes in structural morphology as the composites are formed (i.e. ternary phase formation, grain orientation and size changes) and will be discussed below.

Experimental section

Nanocomposite synthesis

The nanocomposites were prepared using a four-step approach: (i) synthesis of colloidal CdSe nanocrystals (ii) functionalization of the CdSe nanocrystal surface with In_2Se_3 MCC precursor, (iii) controllably adding additional In_2Se_3 MCC precursor, and (iv) decomposing the In_2Se_3 MCC precursor into a polycrystalline In_2Se_3 matrix that encapsulates the nanocrystals.

The In_2Se_3 MCC was made by reacting In_2Se_3 with Se and N_2H_4 to form $(N_2H_4)_2(N_2H_5)_2In_2Se_4$. We confirmed the decomposition conditions for transforming this precursor into In_2Se_3 using thermogravimetric analysis. We heated the precursor to 350 °C, applied a 30 minute isotherm, and then continued to heat the precursor to 450 °C (Fig. 1). The lack of mass loss after the 350 °C isotherm indicates that the thermal

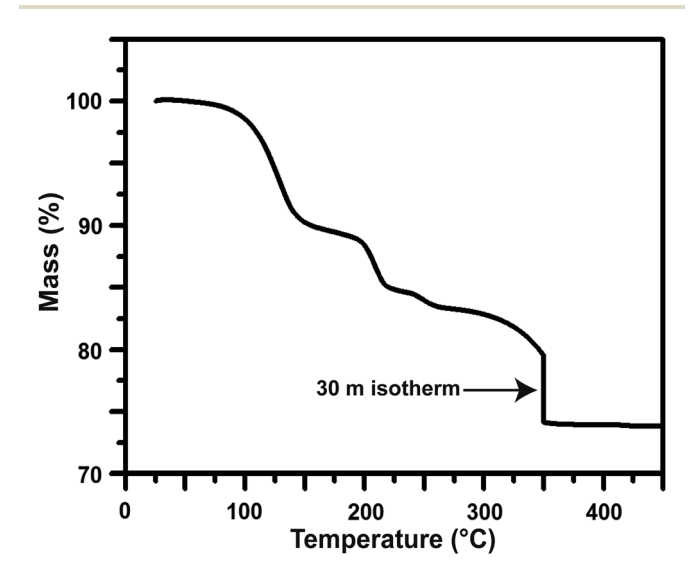


Fig. 1 Thermogravimetric analysis of the In_2Se_3 MCC precursor, $(N_2-H_4)_2(N_2H_5)_2In_2Se_4$. The temperature ramp rate was 2 °C min⁻¹ and a 30 minute isotherm was applied at 350 °C.

decomposition process was complete. Composites consisting of 100% In₂Se₃ were made by directly using this precursor.

Wurtzite phase CdSe nanocrystals were synthesized by the hot injection method reported by Qu et al.54 As synthesized the CdSe nanocrystal surface is passivated by a combination of stearic acid (SA) and trioctylphosphine oxide (TOPO) ligands. These organic ligands were exchanged with the In₂Se₃ MCC precursor using the phase transfer process described by Kovalenko et al.21 Two immiscible solutions, CdSe nanocrystals in hexane and MCC precursor in hydrazine, were combined and stirred for several hours. During this process, the hydrazine phase changed from colorless to dark, indicating the presence of CdSe nanocrystals functionalized with In₂Se₃ MCC precursor. The CdSe nanocrystals were then precipitated several times to separate them from unbound In₂Se₃ MCC precursor. Nanocomposites that are ~100% CdSe were made by directly using this nanocrystal solution. Nanocomposites with lower nanoparticle volume fractions were made by re-introducing appropriate amounts of In₂Se₃ MCC precursor back into the CdSe nanocrystal solution. A detailed report on the nanocomposite synthesis is available in the ESI.†

The elemental composition of the composite was determined by a combination of RBS and PIXE. Since the CdSe nanocrystals and In₂Se₃ matrix in the composite reacted to form a third phase, CdIn₂Se₄, this elemental composition information cannot definitively determine the CdSe volume fraction in the composite (see XRD discussion). Consequently we identify our composites by their In₂: Cd ratio. In the absence of CdIn₂Se₄ formation, a 40:60 ratio implies a composite that is 40 mol% In₂Se₃ and 60 mol% CdSe. Since the CdSe nanocrystal surface was functionalized with In₂Se₃ MCC precursor, the \sim 100% CdSe composites have trace amounts of In.

Thermal conductivity measurements

Thermal conductivity measurements were conducted using the differential 3ω method. 55-57 Nanocomposite samples were prepared by spin-coating the CdSe nanocrystal - In₂Se₃ MCC precursor solution onto silicon substrates and then thermally decomposing the In₂Se₃ MCC precursor at 350 °C for 30 minutes. The sample film thickness generally ranged from 50-130 nm. A 50 nm Al₂O₃ dielectric layer was first deposited on top of the nanocomposite film using electron beam evaporation. 150 nm thick Al 3ω lines were then patterned on top of the dielectric layer using standard lithographic techniques. Line dimensions were generally 500-1000 µm long and 5-6 µm wide, however line widths up to 20 µm were occasionally used. A Keithley 6221 was used as the current source and a Stanford Research Systems SR830 lock-in amplifier was used to measure the 1st and 3rd harmonics of the voltage signal. The temperature coefficient of resistance of the 3ω lines were measured using a custom-built temperature-controlled sample stage. The nanocomposite film thickness was measured by profilometry prior to deposition of the 50 nm Al₂O₃ dielectric layer.

Since the 3ω method measures the combined thermal response of the dielectric layer, nanocomposite film, and substrate, identical reference samples consisting of only the dielectric layer and substrate were prepared simultaneously with the nanocomposite samples. Subtracting the thermal response of the reference sample from the measurement samples enables the nanocomposite thermal conductance to be isolated.

Results and discussion

Nanocomposite structure

The TEM images (Fig. 2) reveal that the nanocomposite consists of randomly dispersed nanoparticles embedded in a matrix. While the general nanoparticle shape is retained throughout the composite formation, we do observe a slight increase in

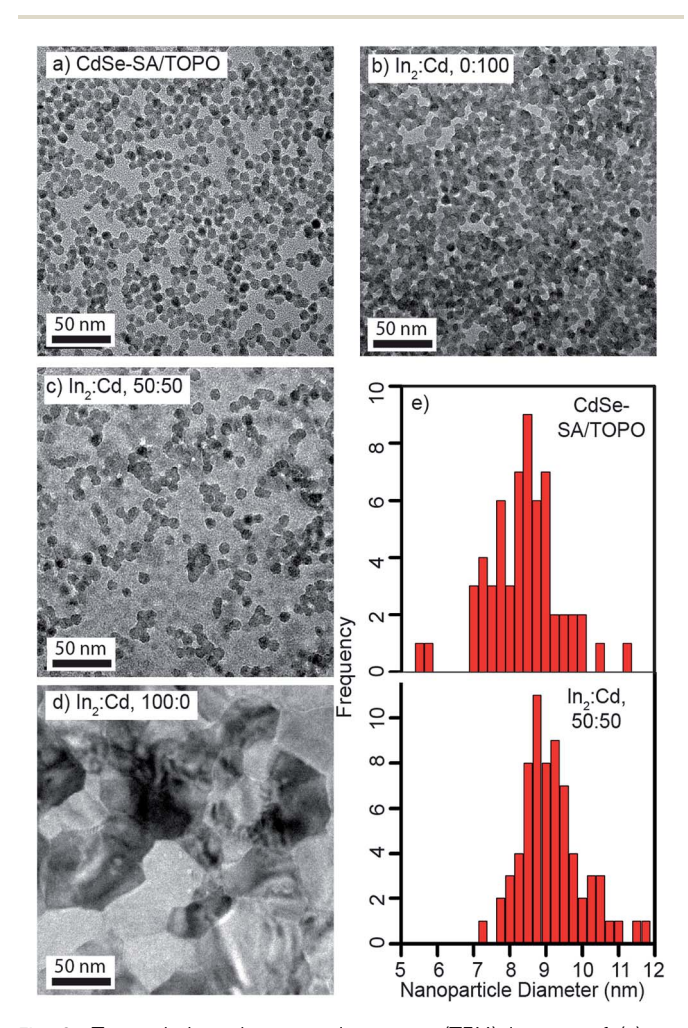


Fig. 2 Transmission electron microscopy (TEM) images of (a) assynthesized colloidal CdSe nanocrystals with a combination of stearic acid (SA) and trioctylphosphine oxide (TOPO) ligands and nanocomposites with In₂: Cd ratios of (b) 0:100, (c) 50:50, and (d) 100 : 0. Histograms illustrating the nanoparticle size distribution for the as-synthesized nanocrystals and the 50:50 composite are shown in part (e). The images in parts (b), (c), and (d) are of samples that have had their MCC precursor converted into In₂Se₃ by annealing at 350 °C for 30 minutes. The background contrast in images (a), (b), and (c) correspond to the carbon support film of the TEM grid, the Si₃N₄ TEM membrane, and γ -In₂Se₃ matrix, respectively. Energy dispersive X-ray spectroscopy data illustrating the elemental composition variations between the nanoparticles and matrix is available in Fig. S2 of the ESI.†

nanoparticle size after composite formation. The average diameter of the as-synthesized CdSe nanocrystals is 8.2 nm (Fig. 2a and e) whereas the average nanoparticle diameter in the 50:50 composite is 9.0 nm (Fig. 2c and e). We believe this slight growth in nanoparticle size is due to the formation of CdIn $_2$ Se $_4$ at the interface between the CdSe nanocrystal and the In $_2$ Se $_3$ matrix (see XRD discussion). In the absence of CdSe nanocrystals, the formation of relatively large In $_2$ Se $_3$ grains is observed (38 \pm 12 nm, Fig. 2d).

The SEM images (Fig. 3) show that mass loss and densification during thermal conversion of the MCC precursor into In₂Se₃ lead to mesoporosity in the nanocomposites. This mesoporosity was also evident when comparing film thicknesses measured via RBS and profilometry; profilometry thicknesses were approximately 20% greater than thicknesses determined by RBS, which assume fully dense films (Fig. S5 and S6†). Structural features on the order of 10¹ and 10² nm in size are visible in the SEM images of 100% In₂Se₃ (Fig. 3d). By comparison with the TEM images, we believe the 10¹ nm-scale features correspond to the In₂Se₃ grains whereas the 10² nmscale features correspond to defects formed during thermal decomposition of the MCC precursor. Although the SEM images exhibit a rich surface structure, the nanocomposite films were optically smooth. Film roughnesses were generally less than 10 nm as measured by atomic force microscopy.

XRD of the decomposed $\rm In_2Se_3$ MCC precursor indicates the formation of $\gamma\text{-In}_2Se_3$ (Fig. 4b), which is one of many $\rm In_2Se_3$ polymorphs. 58 $\gamma\text{-In}_2Se_3$ has a defect wurtzite structure with 1/3 of the In sites vacant. 58,59 Due to surface effects, it can be anticipated that the formation of thin film samples may exhibit

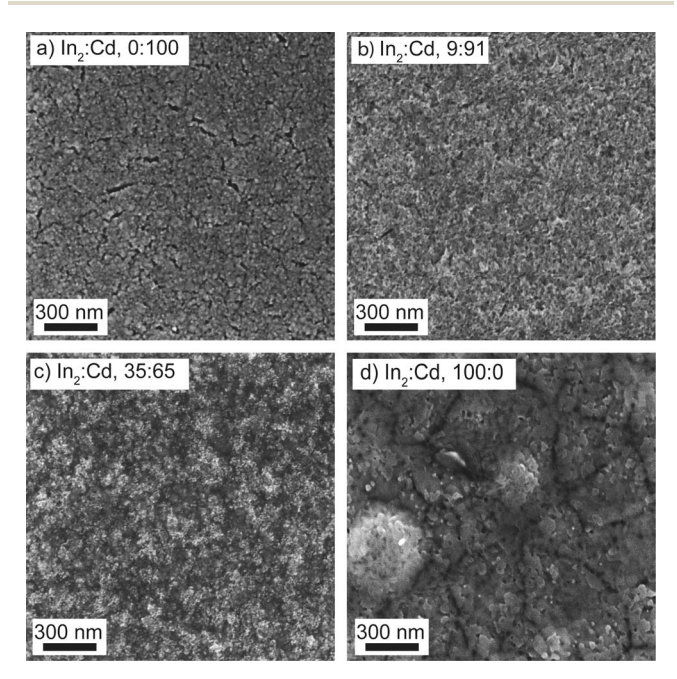


Fig. 3 Scanning electron microscopy images of nanocomposites with ln_2 : Cd ratios of (a) 0:100, (b) 9:91, (c) 35:65, and (d) 100:0. Energy dispersive X-ray spectroscopy data illustrating the microscale chemical homogeneity of the sample is available in Fig. S3 of the ESI.†

morphological changes relative to powder samples. This effect is clearly observed when thermally decomposing In_2Se_3 MCC powder relative to spin-coated In_2Se_3 MCC thin films (Fig. 4b and c). While the powder sample closely matches the γ - In_2Se_3 powder diffraction file, the thin film sample exhibits only a single diffraction peak corresponding to (0 0 6). This indicates that the grains in the γ - In_2Se_3 thin films preferentially orient themselves with the ab-plane parallel to the substrate. We are unaware of any literature reports on the surface energy of γ - In_2Se_3 , but believe that these growth characteristics imply that the surface energy of γ - In_2Se_3 has significant crystallographic anisotropy. Since it is thermodynamically preferable for the γ - In_2Se_3 to minimize its free energy during growth, our observed

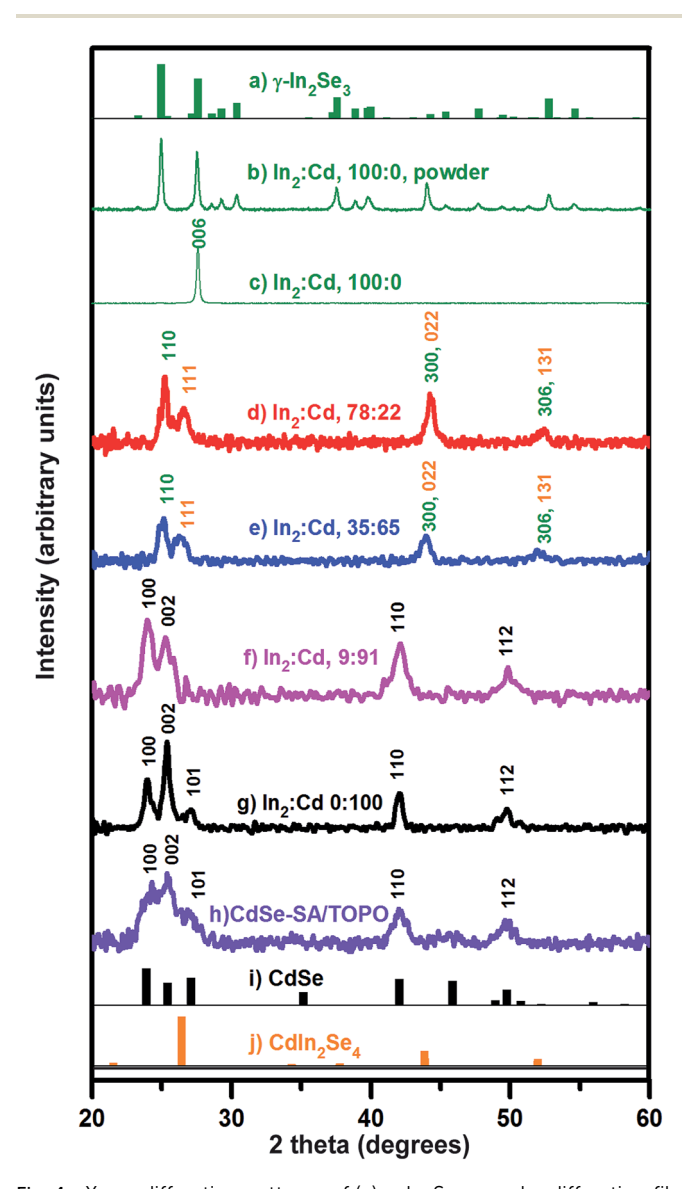


Fig. 4 X-ray diffraction patterns of (a) $\gamma\text{-In}_2\text{Se}_3$ powder diffraction file 01-089-0658, (b) $\gamma\text{-In}_2\text{Se}_3$ powder, thin film nanocomposites with In $_2$: Cd ratios of (c) 100 : 0, (d) 78 : 22, (e) 35 : 65, and (f) 9 : 91, (g) 0 : 100 (h) as-synthesized colloidal CdSe nanocrystals with a combination of stearic acid (SA) and trioctylphosphine oxide (TOPO) ligands, (i) CdSe powder diffraction file 01-077-0021, and (j) CdIn $_2\text{Se}_4$ powder diffraction file 00-056-1124.

growth characteristics imply that the low- and high-energy crystal facets of γ -In₂Se₃ are parallel and perpendicular to the ab-plane, respectively. By growing with the ab-plane parallel to the substrate, the surface area of the high-energy facets was minimized. It is worth noting that another common form of indium selenide, α -In₂Se₃, is also known to be highly anisotropic.^{58,60}

The strong crystallographic orientation preference of the In₂Se₃ is eliminated upon introducing CdSe nanocrystals into the composite, which indicates that the CdSe nanocrystals have a highly disruptive effect on the In₂Se₃ formation. This is indicated by the disappearance of the (0 0 6) In₂Se₃ reflection and appearance of new In₂Se₃ reflections. The large decrease in the signal-noise ratio of the XRD pattern upon inclusion of CdSe nanocrystals also indicates that the resulting In₂Se₃ grains are much smaller than in the 100% In₂Se₃ samples. This formation of smaller grains is corroborated by TEM images of the composites; In₂Se₃ grains are clearly resolved in the 100% In₂Se₃ images, but are not resolved upon introduction of CdSe nanocrystals (Fig. 2c and d). This change in In₂Se₃ formation is likely due to the CdSe nanocrystals functioning as nucleation sites for In₂Se₃ crystallites. It is intuitive that the orientation of In₂Se₃ grains is random in the composites containing CdSe nanocrystals because the orientations of the CdSe nanocrystals themselves are randomized during deposition of the CdSe nanocrystal-MCC precursor mixture. It is also intuitive that the In₂Se₃ grain sizes are smaller in these composites because the presence of CdSe nanocrystals inhibits the formation of the large grains observed in the 100% In₂Se₃ samples.

The observed CdSe diffraction peak widths in our composites demonstrate that the In₂Se₃ matrix inhibits CdSe nanocrystal merger and growth (Fig. 4f-h). The broad peaks of the assynthesized CdSe nanocrystals with organic ligands become notably sharper in the \sim 100% CdSe nanocomposite, which is indicative of an increase in CdSe crystallite size. 61 Scherrer analysis of the (1 1 0) peak in the as-synthesized CdSe colloidal nanocrystals and the \sim 100% CdSe composite yield grain sizes of 8 nm and 20 nm, respectively. This increase in crystallite size is also visible in the TEM images, which show a significant amount of nanocrystal fusing (Fig. 2b). This crystallite growth is not surprising given the lack of matrix in between nanocrystals and the relatively high 350 °C annealing temperatures used to make the composites. However, even a modest inclusion of In₂Se₃ into the composite, such as that of the 9:91 sample (Fig. 4f), yields a noticeable decrease in CdSe diffraction peak sharpening. Scherrer analysis of the (1 1 0) peak in the 9:91 sample yields a grain size of 11 nm.

XRD characterization reveals the formation of a ternary phase, CdIn₂Se₄, in the nanocomposites and suggests a rich interaction between the CdSe nanocrystals and the In₂Se₃ matrix. Notably, only In₂Se₃ and CdIn₂Se₄ are observed in some of our XRD patterns (Fig. 4d and e). While this qualitatively suggests the complete conversion of CdSe nanocrystals into CdIn₂Se₄ nanocrystals, such a conclusion would be oversimplified. For example, while our 35:65 sample shows only In₂Se₃ and CdIn₂Se₄ XRD peaks (Fig. 4e), it is stoichiometrically impossible for this sample to only form these compounds;

stoichiometry would instead dictate the formation of CdSe and CdIn₂Se₄. This peculiarity can be explained by calculating the relative XRD peak intensities for CdSe and CdIn₂Se₄, which demonstrates that X-ray diffraction from CdIn₂Se₄ is inherently more intense than CdSe. The intensity of a XRD peak is proportional to $|S_{hkl}|^2 M_{hkl}/V_c^2$ where S_{hkl} and M_{hkl} are the structure factor and multiplicity factor of the hkl peak and V_c is the unit cell volume. Yalues for the structure factor and multiplicity factor come from analysis of the crystallographic unit cell and symmetry, respectively. Calculation of these values show that the $(1\ 1\ 1)$ peak of CdIn₂Se₄ is more intense than the $(0\ 0\ 2)$ and $(1\ 0\ 0)$ peaks of CdSe by factors of 3.7 and 6.8, respectively (see ESI†). Consequently it is not surprising that we can observe CdIn₂Se₄ diffraction without CdSe diffraction.

As mentioned in the earlier TEM discussion, the slight nanocrystal diameter growth from 8.2 nm to 9.0 nm in the 50: 50 sample suggests the formation of a thin CdIn₂Se₄ layer at the interface between the CdSe nanocrystals and In₂Se₃ matrix. It is worth noting that the conversion of 8.2 nm CdSe nanocrystals into CdIn₂Se₄ via the addition of In and Se would result in 12.6 nm diameter nanocrystals, which are clearly not present in our TEM images. Nonetheless, it would still be possible to get 9.0 nm diameter CdIn₂Se₄ nanocrystals if Cd diffuses into the In₂Se₃ matrix. Consequently, while we believe a thin CdIn₂Se₄ layer between the CdSe nanocrystals and In2Se3 matrix is the most likely scenario, this cannot be definitively determined with the present data. Should the formation of ternary phases wish to be avoided, the use of other nanocrystal-matrix combinations with appropriate phase behavior could be used; for example, CdSe and SnSe2 do not form ternary phases. 62 MCC precursors with low temperature decompositions such as that correspond to SnS2,63 Cu2S,64 or ZnTe65 could also be used to limit elemental interdiffusion between the nanoparticles and matrix.

Nanocomposite thermal transport

Thermal transport in nanostructured materials is of interest for applications ranging from thermoelectricity, thermal barrier coatings, electronics thermal management, phase change memory, and heat assisted magnetic recording.66 The structural motif of nanoparticles embedded in a crystalline matrix is a common theme in the thermal sciences community. 1-5,7,45,46 It is well known that matrix-embedded nanoparticles promote broadband scattering of phonons, which correspondingly leads to low thermal conductivities. This is particularly important for thermoelectric applications wherein reduced thermal conductivities lead to large improvements in energy conversion efficiency.1-5,7 Notably CdSe alloyed with Hg has been investigated for its thermoelectrics properties.^{67,68} In addition, a stoichiometric variant of indium selenide, In₄Se₃, is one of the best bulk thermoelectric materials.⁶⁹ Inspired by these facts, we measured the thermal conductivity of our composites.

Fig. 5 shows the room temperature thermal conductivity of the nanocomposites as a function of In_2 : Cd ratio. For reference purposes, the upper horizontal axis of Fig. 5 indicates the CdSe volume fraction in the limit of negligible CdIn₂Se₄

formation. The 100% In_2Se_3 and \sim 100% CdSe samples have average thermal conductivities of 0.32 and 0.53 W m⁻¹ K⁻¹, respectively. Surprisingly, the thermal conductivities of the mixed CdSe- In_2Se_3 composites were insensitive to the amount of CdSe and were \sim 0.3 W m⁻¹ K⁻¹ in all cases. These low thermal conductivities are comparable to amorphous polymers, which is quite remarkable for inorganic crystalline materials. No correlation between measured thermal conductivity and film thickness was observed (Fig. S4†). This indicates that thermal transport in these samples is diffusive and that the thermal contact resistances between layers of the 3ω thermal conductivity samples are negligible.

The thermal conductivity of our nanostructured $\gamma\text{-In}_2Se_3$ is a factor of 3 lower than other reports on polycrystalline $\gamma\text{-In}_2Se_3$. Our lower thermal conductivity can be understood in the context of microstructural differences between our samples and those in the other report. Yim *et al.* The prepared their samples *via* mechanical alloying and spark plasma sintering, which led to an isotropic polycrystalline sample with grain sizes spanning tens to hundreds of nanometers. In contrast, our samples are anisotropic and have relatively monodisperse grain sizes on the order of tens of nanometers. As seen in the TEM images, the lateral grain size of our samples (which, due to their preferential crystallographic orientation, corresponds to *ab*-plane) is 38 ± 12 nm (Fig. 2d). Although we did not directly measure the crossplane grain size, we infer that it is smaller than the lateral grain size as dictated by the Wulff construction. The Wulff

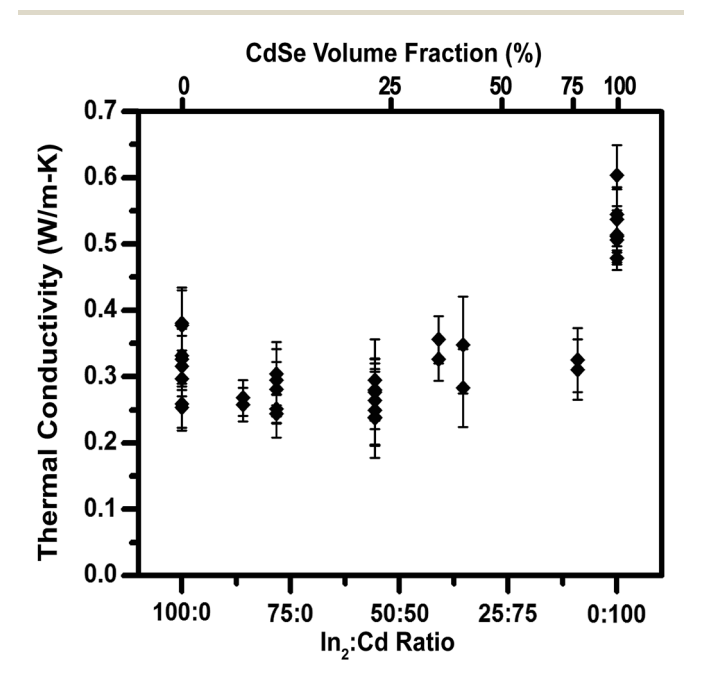


Fig. 5 Thermal conductivity of nanocomposites with varying \ln_2 : Cd ratios. Increasing amounts of Cd correspond to larger nanoparticle volume fractions in the composite. The upper horizontal axis indicates the nanocomposite's CdSe volume fraction in the limit of negligible CdIn₂Se₄ formation. Thermal conductivity measurements were done on multiple films and on up to two locations per film for each \ln_2 : Cd ratio. All data points are shown above to best illustrate sample-to-sample and location-to-location variations.

construction states that crystals grow slowest in directions perpendicular to their low energy surfaces, which in our case means that the smallest grain dimension should be in the crossplane direction. The reduced grain sizes in our γ -In₂Se₃ relative to Yim *et al.*,⁵³ naturally leads to increased phonon scattering and reduced thermal conductivity.

Another factor leading to lower thermal conductivities in our γ-In₂Se₃ measurements is that we are probing transport along the c-axis. Since the low energy crystal facets in γ-In₂Se₃ are parallel to the ab-plane, the weakest bonds should be along the c-axis. This means that the phonon group velocities are slowest along the c-axis and as a consequence, the c-axis should be the crystallographic direction with lowest thermal conductivity. While it would be useful to assess the effect of this anisotropy by comparing to bulk single crystal γ-In₂Se₃ data, we note that thermal conductivity data in the literature is limited to polycrystalline In₂Se₃.^{53,71} We also note that although our measured thermal conductivity for γ-In₂Se₃ is quite low, it is still well above the minimum thermal conductivity predicted by the Cahill-Pohl model.72 The Cahill-Pohl is often used to approximate the thermal conductivity of amorphous materials and is also commonly called the "minimum thermal conductivity model" and the "amorphous limit". The Cahill-Pohl model estimates a lower limit of 0.13 W m⁻¹ K⁻¹ for In_2Se_3 (see ESI†); this is approximately a factor of 2.5 below our measured thermal conductivity and suggests even lower thermal conductivities for γ -In₂Se₃ are possible.

The thermal conductivity of our nanostructured CdSe is a factor of 17 lower than measurements on bulk single crystal CdSe.51,52 In fact, our average thermal conductivity of 0.53 W m⁻¹ K⁻¹ is near that of the Cahill-Pohl model, which predicts a lower limit of 0.40 W m⁻¹ K⁻¹ for CdSe (see ESI†).⁷² A thermal conductivity this low suggests very intense phonon scattering in our ~100% CdSe composites. While thermal conductivity measurements on colloidal nanocrystals are relatively scarce, the existing literature shows that nanocrystal size and surface chemistry are the key factors determining thermal transport. 25,44 Ong et al.44 studied thermal transport in colloidal CdSe nanocrystals with varying surface chemistry and diameters ranging from 3.5-5.2 nm. Feser et al.25 used colloidal nanocrystals to prepare polycrystalline CdSe with controlled grain sizes varying from 3.5-6.2 nm. The thermal conductivities in these prior works were on the order of 10^{-1} W mK⁻¹, which is comparable to our results. However, extrapolating the results of Ong et al. and Feser et al. to the 20 nm grain size of our ~100% CdSe composites would yield thermal conductivity values greater than our measured value. The fact that our samples have larger grains, but a comparable thermal conductivity, implies that phonon scattering at our interfaces is more intense (i.e. our grain boundaries have a lower phonon transmission probability).73 This could be a result of the different CdSe crystallite surface chemistries in our work and these prior works. Feser et al. functionalized their CdSe nanocrystals with HgSe MCC precursor instead of the In2Se3 MCC precursor used in our work. Since CdSe and HgSe form a solid solution,74 the grain boundary interfaces in the work by Feser et al. are very different than ours. While Ong et al. also studied CdSe nanocrystals with

MCC precursor ligands, they did not thermally transform the MCC precursor into a metal-chalcogenide semiconductor and consequently their interfaces also differ from ours. Differences in phonon impurity scattering between our samples and these earlier works could also be affecting thermal transport. It should also be noted that mesoporosity differences in our samples and these prior works might also be leading to thermal transport dissimilarities.

With the exception of the \sim 100% CdSe sample, the thermal conductivities of our nanocomposites were surprisingly insensitive to CdSe volume fraction. The notable increase in thermal conductivity upon reaching ~100% CdSe likely arises from the increase in CdSe grain size that occurs in the absence of an In₂Se₃ matrix. We hypothesize the otherwise insensitive results to CdSe volume fraction arise from a variety of morphological changes that have competing effects on thermal conductivity. Since multiple morphological changes occur simultaneously in our composites, it is difficult to isolate the impact of any one change on thermal transport. Consequently we limit the discussion below to identifying these changes and qualitatively discussing their impact on thermal conductivity.

As CdSe is introduced into the In₂Se₃ matrix, the two most obvious morphological changes are a decrease in In₂Se₃ grain size and elimination of the preferential In₂Se₃ grain orientation. The decrease in In₂Se₃ grain size should reduce thermal conductivity due to increased phonon scattering at grain boundary interfaces. The elimination of the preferential In₂Se₃ grain orientation should increase thermal conductivity due to an increased phonon group velocity in the direction of thermal transport (i.e. as discussed earlier, the growth characteristics of the γ -In₂Se₃ imply that the phonon group velocity is slow along the *c*-axis and fast in the *ab*-plane).

Another important morphological change is the occurrence of CdSe-In₂Se₃ grain boundaries. In the simple case of isotropic crystal structures, one would expect this to reduce thermal conductivity. This is because compositionally-mismatched grain boundaries should have a greater acoustic impedance mismatch than compositionally-matched grain boundaries, which consequently leads to larger thermal interface resistances.73 However, in our case the net effect of CdSe-In₂Se₃ grain boundaries is ambiguous due to the anisotropy of the In₂Se₃ grains. Crystalline anisotropy causes thermal interface resistance to be a function of both composition and grain orientation. This dependency has been both previously modeled75 and experimentally demonstrated.76 Although we could not find literature for the speed of sound anisotropy in γ-In₂Se₃, we note that the speed of sound anisotropy in α -In₂Se₃ is significant, \sim 70% for the longitudinal phonon mode.60 We also note that the acoustic impedance mismatch in our grain boundaries is dominated by the speed of sound since the densities of CdSe and In₂Se₃ only differ by \sim 6%. Due to these grain orientation effects, some fraction of the In₂Se₃-In₂Se₃ grain boundaries likely have larger thermal interface resistances than CdSe-In₂Se₃ grain boundaries and vice versa. Consequently the relative impact of In₂Se₃-In₂Se₃ versus In₂Se₃-CdSe grain boundaries on thermal conductivity is ambiguous.

Yet another important morphological change is the formation of CdIn₂Se₄. As mentioned earlier, this CdIn₂Se₄ likely forms at the interface between the CdSe nanocrystals and the In₂Se₃ matrix, and so would also affect the CdSe-In₂Se₃ thermal interface resistance. If the CdIn₂Se₄ layer is very thin, it can have an interface "smoothing" effect⁷⁷ that decreases thermal interface resistance and thereby increases nanocomposite thermal conductivity. On the other hand, if the CdIn2Se4 is thick enough, two distinct interfaces could arise, CdSe-CdIn₂Se₄ and CdIn₂Se₄-In₂Se₃. The combined thermal resistance of these two interfaces could be larger than that of a single CdSe-In₂Se₃ interface and thereby decrease nanocomposite thermal conductivity.

Regardless of its precise origins, this thermal conductivity insensitivity to CdSe volume fraction suggests that low thermal conductivities can be reliably achieved using this solutionphase synthesis route to nanocomposite materials. Since these thermal conductivities are already attractively low for thermoelectrics, future work measuring the other thermoelectric properties (i.e. electrical conductivity and Seebeck coefficient) is merited. Furthermore, studies using the recently-developed colloidal nanocrystal chemistries that yield charge mobilities near single-crystal values would be especially promising.35

Conclusions

The synthesis and characterization of nanocomposites with variable nanoparticle volume fraction made by combining CdSe nanocrystals and In₂Se₃ MCC precursor has been presented. We observe rich structural and chemical interactions between the CdSe nanocrystals and the In₂Se₃ matrix during composite formation. These interactions include alterations in In₂Se₃ grain size and orientation as well as the formation of a ternary phase, CdIn₂Se₄. The thermal conductivity of these composites is on the order of 10^{-1} W m⁻¹ K⁻¹ over the entire nanoparticle volume fraction range, which is remarkably low for inorganic crystalline materials and is comparable to amorphous polymers. With the exception of the ~100% CdSe samples, the thermal conductivity of the nanocomposite is insensitive to CdSe volume fraction. We attribute this insensitivity to competing effects that arise from structural morphology changes as the composite is formed.

Acknowledgements

This work was supported by the Young Investigator Research Program of the Air Force Office of Scientific Research through award number FA9550-13-1-0163 and by the National Science Foundation through award number CBET-1227979. We gratefully acknowledge the use of facilities within the LeRoy Eyring Center for Solid State Science and Center for Solid State Electronics Research, both of which are located at Arizona State University. We also thank Don Seo, Barry Wilkens, and Emmanuel Soignard for thermogravimetric analysis, RBS and PIXE measurements, and helpful discussions, respectively.

References

- K. Biswas, J. He, I. D. Blum, C. I. Wu, T. P. Hogan,
 D. N. Seidman, V. P. Dravid and M. G. Kanatzidis, *Nature*,
 2012, 489, 414-418.
- 2 M. S. Dresselhaus, G. Chen, M. Y. Tang, R. G. Yang, H. Lee, D. Z. Wang, Z. F. Ren, J. P. Fleurial and P. Gogna, *Adv. Mater.*, 2007, **19**, 1043–1053.
- 3 W. Liu, X. Yan, G. Chen and Z. Ren, *Nano Energy*, 2012, **1**, 42–56.
- 4 N. Mingo, D. Hauser, N. P. Kobayashi, M. Plissonnier and A. Shakouri, *Nano Lett.*, 2009, **9**, 711–715.
- 5 W. Kim, J. Zide, A. Gossard, D. Klenov, S. Stemmer, A. Shakouri and A. Majumdar, *Phys. Rev. Lett.*, 2006, **96**, 045901.
- 6 R. Y. Wang, J. P. Feser, J. S. Lee, D. V. Talapin, R. Segalman and A. Majumdar, *Nano Lett.*, 2008, **8**, 2283–2288.
- 7 K. Biswas, J. Q. He, Q. C. Zhang, G. Y. Wang, C. Uher, V. P. Dravid and M. G. Kanatzidis, *Nat. Chem.*, 2011, 3, 160–166.
- 8 M. Liu, Y. Ma, H. Wu and R. Y. Wang, ACS Nano, 2015, 9, 1341–1351.
- 9 M. L. Liu and R. Y. Wang, Nanoscale, 2013, 5, 7234-7237.
- D. V. Talapin, J. S. Lee, M. V. Kovalenko and E. V. Shevchenko, *Chem. Rev.*, 2010, 110, 389–458.
- 11 C. H. M. Chuang, P. R. Brown, V. Bulovic and M. G. Bawendi, Nat. Mater., 2014, 13, 796–801.
- 12 M. A. Caldwell, R. G. D. Jeyasingh, H. S. P. Wong and D. J. Milliron, *Nanoscale*, 2012, 4, 4382–4392.
- 13 S. H. Sun, C. B. Murray, D. Weller, L. Folks and A. Moser, *Science*, 2000, **287**, 1989–1992.
- 14 A. Llordes, G. Garcia, J. Gazquez and D. J. Milliron, *Nature*, 2013, 500, 323–326.
- E. L. Runnerstrom, A. Llordes, S. D. Lounis and D. J. Milliron, *Chem. Commun.*, 2014, 50, 10555–10572.
- 16 B. O. Dabbousi, M. G. Bawendi, O. Onitsuka and M. F. Rubner, *Appl. Phys. Lett.*, 1995, **66**, 1316–1318.
- 17 T. Trindade, M. C. Neves and A. M. V. Barros, *Scr. Mater.*, 2000, 43, 567–571.
- 18 M. Guglielmi, A. Martucci, E. Menegazzo, G. C. Righini, S. Pelli, J. Fick and G. Vitrant, J. Sol-Gel Sci. Technol., 1997, 8, 1017–1021.
- 19 T. Mokari, H. Sertchook, A. Aharoni, Y. Ebenstein, D. Avnir and U. Banin, *Chem. Mater.*, 2005, **17**, 258–263.
- 20 A. Llordes, A. T. Hammack, R. Buonsanti, R. Tangirala, S. Aloni, B. A. Helms and D. J. Milliron, *J. Mater. Chem.*, 2011, 21, 11631–11638.
- 21 M. V. Kovalenko, M. Scheele and D. V. Talapin, *Science*, 2009, 324, 1417–1420.
- 22 R. Tangirala, J. L. Baker, A. P. Alivisatos and D. J. Milliron, Angew. Chem., Int. Ed., 2010, 49, 2878–2882.
- 23 D. B. Mitzi, M. Copel and S. J. Chey, Adv. Mater., 2005, 17, 1285–1289.
- 24 D. J. Milliron, S. Raoux, R. Shelby and J. Jordan-Sweet, *Nat. Mater.*, 2007, **6**, 352–356.
- 25 J. P. Feser, E. M. Chan, A. Majumdar, R. A. Segalman and J. J. Urban, *Nano Lett.*, 2013, 13, 2122–2127.

- 26 D. B. Mitzi, Adv. Mater., 2009, 21, 3141-3158.
- 27 A. Nag, H. Zhang, E. Janke and D. V. Talapin, *Z. Phys. Chem.* (*Muenchen, Ger.*), 2015, **229**, 85–107.
- 28 A. Nag, M. V. Kovalenko, J. S. Lee, W. Liu, B. Spokoyny and D. V. Talapin, *J. Am. Chem. Soc.*, 2011, **133**, 10612–10620.
- 29 H. Zhang, J. Jang, W. Liu and D. V. Talapin, *ACS Nano*, 2014, **8**, 7359–7369.
- 30 W. Liu, J. S. Lee and D. V. Talapin, J. Am. Chem. Soc., 2013, 135, 1349–1357.
- 31 D. K. Ko, Y. Kang and C. B. Murray, *Nano Lett.*, 2011, **11**, 2841–2844.
- 32 J. H. Choi, A. T. Fafarman, S. J. Oh, D. K. Ko, D. K. Kim, B. T. Diroll, S. Muramoto, J. G. Gillen, C. B. Murray and C. R. Kagan, *Nano Lett.*, 2012, 12, 2631–2638.
- 33 D. S. Chung, J. S. Lee, J. Huang, A. Nag, S. Ithurria and D. V. Talapin, *Nano Lett.*, 2012, 12, 1813–1820.
- 34 J. S. Lee, M. V. Kovalenko, J. Huang, D. S. Chung and D. V. Talapin, *Nat. Nanotechnol.*, 2011, **6**, 348–352.
- 35 D. S. Dolzhnikov, H. Zhang, J. Jang, J. S. Son, M. G. Panthani, T. Shibata, S. Chattopadhyay and D. V. Talapin, *Science*, 2015, 347, 425-428.
- 36 D. K. Kim, Y. Lai, B. T. Diroll, C. B. Murray and C. R. Kagan, Nat. Commun., 2012, 3, 1216.
- 37 H. J. Yun, T. Paik, M. E. Edley, J. B. Baxter and C. B. Murray, *ACS Appl. Mater. Interfaces*, 2014, **6**, 3721–3728.
- 38 D. Yang, C. Lu, H. Yin and I. P. Herman, *Nanoscale*, 2013, 5, 7290–7296.
- 39 Y. Zhang, M. L. Snedaker, C. S. Birkel, S. Mubeen, X. Ji, Y. Shi, D. Liu, X. Liu, M. Moskovits and G. D. Stucky, *Nano Lett.*, 2012, 12, 1075–1080.
- 40 M.-K. Han, S. Kim, H.-Y. Kim and S.-J. Kim, *RSC Adv.*, 2013, 3, 4673.
- 41 D. Cadavid, M. Ibáñez, A. Shavel, O. J. Durá, M. A. López de la Torre and A. Cabot, *J. Mater. Chem. A*, 2013, **1**, 4864.
- 42 M. V. Kovalenko, B. Spokoyny, J. S. Lee, M. Scheele, A. Weber, S. Perera, D. Landry and D. V. Talapin, *J. Am. Chem. Soc.*, 2010, **132**, 6686–6695.
- 43 R. Y. Wang, R. Tangirala, S. Raoux, J. L. Jordan-Sweet and D. J. Milliron, *Adv. Mater.*, 2012, **24**, 99–103.
- 44 W. L. Ong, S. M. Rupich, D. V. Talapin, A. J. McGaughey and J. A. Malen, *Nat. Mater.*, 2013, **12**, 410–415.
- 45 G. Pernot, M. Stoffel, I. Savic, F. Pezzoli, P. Chen, G. Savelli, A. Jacquot, J. Schumann, U. Denker, I. Monch, C. Deneke, O. G. Schmidt, J. M. Rampnoux, S. Wang, M. Plissonnier, A. Rastelli, S. Dilhaire and N. Mingo, *Nat. Mater.*, 2010, 9, 491–495.
- 46 W. Kim, R. Wang and A. Majumdar, *Nano Today*, 2007, **2**, 40–47.
- 47 B. Poudel, Q. Hao, Y. Ma, Y. Lan, A. Minnich, B. Yu, X. Yan, D. Wang, A. Muto, D. Vashaee, X. Chen, J. Liu, M. S. Dresselhaus, G. Chen and Z. Ren, *Science*, 2008, 320, 634–638.
- 48 H. Lee, Y. Lan, X. W. Wang, G. Zhu, M. S. Dresselhaus, G. Chen and Z. Ren, *Nano Lett.*, 2008, **8**, 4670–4674.
- 49 H. Zhang and A. J. Minnich, Sci. Rep., 2015, 5, 8995.

- 50 S. LeBlanc, S. K. Yee, M. L. Scullin, C. Dames and K. E. Goodson, Renewable Sustainable Energy Rev., 2014, 32, 313 - 327
- 51 A. V. Ioffe and A. F. Ioffe, Soviet Physics-Solid State, 1960, 2, 719-728.
- 52 G. A. Slack, Phys. Rev. B: Solid State, 1972, 6, 3791-3800.
- 53 J.-H. Yim, H.-H. Park, H. W. Jang, M.-J. Yoo, D.-S. Paik, S. Baek and J.-S. Kim, J. Electron. Mater., 2012, 41, 1354–1359.
- 54 L. H. Qu, Z. A. Peng and X. G. Peng, Nano Lett., 2001, 1, 333-
- 55 T. Borca-Tasciuc, A. R. Kumar and G. Chen, Rev. Sci. Instrum., 2001, 72, 2139-2147.
- 56 D. G. Cahill, Rev. Sci. Instrum., 1990, 61, 802-808.
- 57 S. M. Lee and D. G. Cahill, *J. Appl. Phys.*, 1997, **81**, 2590–2595.
- 58 G. Han, Z. G. Chen, J. Drennan and J. Zou, Small, 2014, 10, 2747-2765.
- 59 J. P. Ye, S. Soeda, Y. Nakamura and O. Nittono, Jpn. J. Appl. Phys., Part 1, 1998, 37, 4264-4271.
- 60 N. D. Raranskii, V. N. Balazyuk, Z. D. Kovalyuk, N. I. Mel'nik and V. B. Gevik, Inorg. Mater., 2011, 47, 1174-1177.
- 61 J. Howe and B. Fultz, Transmission Electron Microscopy and Diffractometry of Materials, Springer, New York, 3rd edn, 2008.
- 62 E. A. Galiulin, I. N. Odin and A. V. Novoselova, Zh. Neorg. Khim., 1982, 27, 266-268.
- 63 D. B. Mitzi, L. L. Kosbar, C. E. Murray, M. Copel and A. Afzali, Nature, 2004, 428, 299-303.
- 64 D. B. Mitzi, Inorg. Chem., 2007, 46, 926-931.

- 65 D. B. Mitzi, Inorg. Chem., 2005, 44, 7078-7086.
- 66 D. G. Cahill, P. V. Braun, G. Chen, D. R. Clarke, S. H. Fan, K. E. Goodson, P. Keblinski, W. P. King, G. D. Mahan, A. Majumdar, H. J. Maris, S. R. Phillpot, E. Pop and L. Shi, Appl. Phys. Rev., 2014, 1, 011305.
- 67 E. Cruceanu and S. Ionescub, J. Mater. Sci., 1969, 4, 570-573.
- 68 J. O. Sofo, J. Appl. Phys., 1995, 77, 1561-1563.
- 69 J. S. Rhyee, K. H. Lee, S. M. Lee, E. Cho, S. Il Kim, E. Lee, Y. S. Kwon, J. H. Shim and G. Kotliar, Nature, 2009, 459, 965-968.
- 70 G. Wulff, Zeitschrift für Krystallographie und Mineralogie, 1901, 34, 449-530.
- 71 N. N. Sirota and L. I. Berger, *Inzh.-Fiz. Zh.*, 1958, 1, 117–120.
- 72 D. G. Cahill, S. K. Watson and R. O. Pohl, Phys. Rev. B: Condens. Matter Mater. Phys., 1992, 46, 6131-6140.
- 73 E. T. Swartz and R. O. Pohl, Rev. Mod. Phys., 1989, 61, 605-668.
- 74 N. P. Gavaleshko, P. N. Gorlei, S. Y. Paranchich, V. M. Frasunyak and V. V. Khomyak, Inorg. Mater., 1983, 19, 298-300.
- 75 J. C. Duda, J. L. Smoyer, P. M. Norris and P. E. Hopkins, Appl. Phys. Lett., 2009, 95, 031912.
- 76 P. E. Hopkins, T. Beechem, J. C. Duda, K. Hattar, J. F. Ihlefeld, M. A. Rodriguez and E. S. Piekos, Phys. Rev. B: Condens. Matter Mater. Phys., 2011, 84, 125408.
- 77 T. S. English, J. C. Duda, J. L. Smoyer, D. A. Jordan, P. M. Norris and L. V. Zhigilei, Phys. Rev. B: Condens. Matter Mater. Phys., 2012, 85, 035438.